Visualizing the Gibbs Models†

Kenneth R. Jolls*

Department of Chemical and Biological Engineering, Iowa State University, Ames, Iowa 50011

Daniel C. Coy

Computational Fluid Dynamics, BP Refinery Technology, Naperville, Illinois 60563

Images of thermodynamic fundamental and state functions for pure, binary, and ternary systems have been created using high-performance computer graphics. Results were obtained from integrations of the Peng−Robinson equation, using standard heat-capacity data and common mixing rules. The Legendre-transform basis of the various thermodynamic coordinate systems is demonstrated, and the agreement between those geometries and the relevant criteria for thermodynamic stability is noted. The capacity of the images to convey the nature and utility of complex thermodynamic quantities is used as an argument for greater emphasis on visualization.

Pictures Versus Numbers

Computer visualization can bridge a gap that has existed throughout the history of human enlightenment—that which separates left thinkers and right thinkers. It can enrich the rigid, sequential world of the former while adding quantity and structure to the intuitive meanderings of the latter. It can provide subjective models of very precise ideas while offering analytical interpretations of the purest art.

Educators have long needed visual tools, but they may not welcome modern graphics. As with many high-tech advances, it is urged upon us with such overkill that the wary scholar may be turned away. Confronted by slick videos and animated advertisements selling everything from absinthe to zirconia, the careful teacher may hesitate, wondering understandably if visualized instruction is not just a fancy toy in search of legitimacy.

But famous minds have spoken otherwise. Aristotle said "the soul never thinks without an image".[1] Albert Einstein often did poorly as a conventional student but ultimately became a daydreamer who played with images in his mind—images that were to transform our view of the physical world. The young Winston Churchill lagged similarly behind his schoolmates but later became a master orator with a preference for visual−spatial modes of thought. It took George Patton five years to graduate from West Point—he was clumsy, accident-prone, and so inept at spelling and punctuation that his wife had to correct his writings. But he had a special feeling for timing and spatial relationships that are credited for his legendary skill as a commanding general.[2]

With one-quarter of the human cerebral cortex committed to vision, it would seem that any method sending more data through the visual port would be an important advance. Many of us have had moments when words and numbers failed, and only a picture—perhaps the merest sketch or the most casual graphic—could fill the void to make the point we were trying to express. Cornell's Donald Greenberg said it well while sidestepping the cliché: "A picture is worth 1024 words".[3]

Yet, visualization is not emphasized in modern education.[4] Some see it as an invasion of the traditional ways.[5] Educators can be conservative and reluctant to change time-tested methods. Schemes that have worked well in the past extrapolate effortlessly into the future and pose stubborn obstacles to change.

Our cumulative years of engineering experience have shown us the product of society's left-biased education: bright, hard-working minds focused on a rigid, numerical interpretation of nature—students for whom an equation conveys little more than symbols and numbers to be solved for yet more symbols and more numbers. The global aspects of functional dependence, spatial relationship, and overall cause and effect have all too frequently played a minor role.

And that mindset perpetuates itself. Students from this tradition become professors of like mind. Pedagogies become sacred cows guarded by suspicion and indifference. When such attitudes are mixed with the pressures placed upon today's academic, the result can be a fixed educational paradigm, resistant to change.

But science and engineering have important visual components. Who would teach calculus without showing slopes and areas? Who would teach transport phenomena without picturing flow fields and temperature gradients? Who would talk about sine waves without sketching those familiar, undulating curves? The notions of cause and effect that we pursue in science are universal and separate from the numerical measures we ascribe to them. It is our great loss when the mechanics of obtaining those measures obscure the reasons for doing so.

Righting What's Left

Few disciplines are as consistently left-interpreted as thermodynamics. Almost seven generations of students and teachers have struggled through its subtle, postulated logic since its formalization by J. Willard Gibbs in the early 1870s.[6–8] Thermodynamics has stirred many to write, to philosophize, to preach, to laugh—even to scoff. Yet, in any scientific popularity poll, it is certain to emerge the uncontested loser!

Taken purely from the left, Gibbs' methods translate into an austere formalism of variables and equations—perfect fodder

* To whom correspondence should be addressed. E-mail address: jolls@iastate.edu.

† This paper is dedicated to the memory of Dr. Michael M. Abbott, Professor of Chemical Engineering at Rensselaer Polytechnic Institute, and coauthor with H. C. Van Ness and J. M. Smith of the well-known thermodynamics textbook mentioned in ref 35. Dr. Abbott was a wise scholar, a sensitive humanist, a devoted family person, and a valued friend to all who knew him. We are better for him having been among us.

10.1021/ie071277b CCC: $40.75
Published on Web 07/30/2008

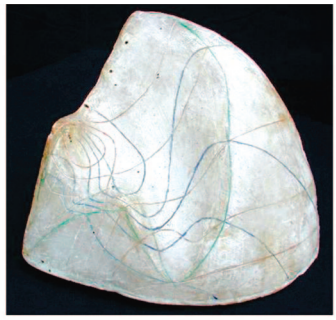

Maxwell's model of the energy-entropy-volume function for water (Cambridge Univ., 1874) — "a fancy surface showing the solid, liquid, and gaseous states."

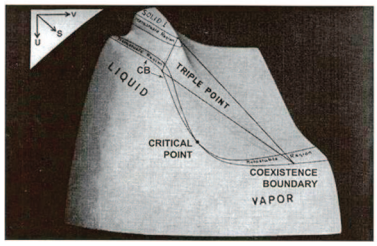

A more accurate model of the same properties by Clark and Katz (Queen's Univ., 1939).

Figure 1. Early models of Gibbs' thermodynamic surface.

for the standard pedagogy through which the subject is often presented. But the birth of that formalism also had a visual element. The vehicle that Gibbs used to connect the laws of thermodynamics with their consequences was a three-dimensional model that represented his ideas and enabled the operations of thermodynamics to be interpreted through geometric reasoning. Property relationships could be explained based on the changes that are allowed or forbidden by the laws of thermodynamics and confirmed by the spatial behavior of his model. Materials were shown to behave with a logical regularity that was meted out by thermodynamics and made intelligible by Gibbs' geometries.

But Willard Gibbs was no artist, and he described his ideas only in words. It was the 1870s, and technical illustration as we know it today hardly existed. The first actual physical model, which showed the near-mystical energy−entropy−volume function (*USV*), was constructed by James Clerk Maxwell, Gibbs' contemporary and head of the Cavendish Laboratory at Cambridge University.

In his *Theory of Heat* (1875), Maxwell wrote:[9]

"Prof J. Willard Gibbs, of Yale College, U.S., to whom we are indebted for a careful examination of the different methods of representing thermodynamic relations by plane diagrams, has introduced an exceedingly valuable method of studying the properties of a substance by means of a surface."

Maxwell's model represented the properties of the three phases of water, but it was only qualitative. It showed a surface with slopes and curvatures that, according to Gibbs, resulted in regions of stable and unstable thermodynamic behavior consistent with the variance and phase changes that we observe with a pure material. Maxwell made three copies of his model and sent one to Gibbs. His personal copy can be seen today in the Cavendish Laboratory at Cambridge, and the one sent to Gibbs is preserved by the Physics Department at Yale. Figure 1 shows Gibbs' copy and also a later and more accurate version constructed by Clark and Katz.[10]

The elegant geometrical scenario that Gibbs described for identifying the levels of thermodynamic stability and the loci of coexisting phases has been discussed by several authors. For details and history, we refer to one highly regarded biography[11] and also to an article by the first author, "Gibbs and the Art of Thermodynamics".[12]

Gibbs' reasoning and Maxwell's construction opened up an important field of research: the study of phase diagrams.[13–17] [To be correct, a phase diagram is any graphic or model showing relationships among measurable properties (for example, pressure, volume, temperature, or composition). This paper uses the more general term *thermodynamic visualization* for a graphic representation of any property relationship.] No textbook on the subject (and there are hundreds) would seem complete without its mandatory collection of graphs and three-dimensional (3-D) projections showing the usual array of *PVT*, *SPT*, *HSP*, $T-x$ and $H-x$ functions for common pure and mixed systems. The work by Tamás and Pál[14] contains a particularly intriguing set of stereographic drawings for ternary systems—anaglyphs, primarily temperature−composition diagrams for solid−liquid equilibria.

However, manual methods alone are hardly adequate to produce the variety of complex geometrical structures that one encounters in visualizations of thermodynamic functions. The key to portraying such models often hinges upon the ability to show delicate slopes and curvatures, intersections and intercepts, and orientations favorable to the viewer. For modern computer graphics, such operations are commonplace. Converting dense thermodynamic data into a three-dimensional drawing by means of appropriate projection geometry is both simple and fast using current technology. Far-more-complicated displays are daily fare in modern films and on commercial television. Indeed no scholarly task has waited so long but been so well-suited for today's computers than visualization of the Gibbsian thermodynamic models.[18]

Goals

This paper shows computer-generated images of selected Gibbs models—3-D parametric sections of thermodynamic fundamental and state functions for pure, binary, and ternary systems in the vicinity of their vapor−liquid critical points. (The mathematical analysis and the resulting equations used to produce data for the Gibbs models are provided as Supporting Information.) The databases were created from integrations of the Peng−Robinson equation in its pure and mixed forms,[19] combined with standard expressions for ideal-gas heat capacity. The drawings appeared first in the 1993 doctoral dissertation of the second author[20] and also may be seen on the authors' website: "Gibbs Models" (http://www.public.iastate.edu/~jolls).

We have three objectives:

(1) To show the role of the Legendre transform in mapping thermodynamic data among the various coordinate systems suited to its analysis.

(2) To show the regularity with which thermodynamic functions appear when their geometries are visualized.

(3) To show the various regions of thermodynamic stabilty and confirm the agreement between model geometry and stability criteria.

The Legendre Transform in Thermodynamics

In physics lectures at the University of Göttingen in 1929, Max Born confirmed that Gibbs had used the Legendre transform in his organization of thermodynamic information into the many coordinate systems that we use today.[21] Referring to Gibbs' third paper, "On the Equilibrium of Heterogeneous Substances"(see ref 8), we find the familiar equations written in his original symbols as they apply to a closed, pure system:

$$\psi = \epsilon - t\eta \quad \text{(the Helmholtz energy)}$$

$$\chi = \epsilon + p\upsilon \quad \text{(the enthalpy)}$$

$$\zeta = \epsilon - t\eta + p\upsilon \quad \text{(the Gibbs energy)}$$

where ϵ is energy and η is entropy. These are abbreviated expressions for the more-general statements given below.

Legendre transforms for pure systems are familiar and have been described thoroughly by many authors.[22–26] In this paper, we will recognize the common forms, show their spatial geometries, and highlight features of thermodynamic interest. Some of the less-common transforms are shown on the "Gibbs Models" website.

Using modern symbolism to express the energy-explicit form of the Fundamental Equation of Thermodynamics for N moles of a pure system, we write, using fully extensive variables,

$$U = f(S,V,N) \quad \text{(the base function)} \tag{1}$$

taking first Legendre transforms

$$A = U - \left(\frac{\partial U}{\partial S}\right)_{V,N} S \quad \text{(the Helmholtz energy, } f(T,V,N)) \tag{2}$$

$$H = U - \left(\frac{\partial U}{\partial V}\right)_{S,N} V \quad \text{(the enthalpy, } f(S,P,N)) \tag{3}$$

taking a second transform,

$$G = U - \left(\frac{\partial U}{\partial S}\right)_{V,N} S - \left(\frac{\partial U}{\partial V}\right)_{S,N} V \quad \text{(the Gibbs energy, } f(T,P,N) \tag{4}$$

To be thorough, one additional first transform and two additional second transforms may be taken for the pure-component case, all involving the variable N. However, for our purposes, little is gained by doing so, and the most useful forms remain the familiar ones that have been given previously. Because eq 1 is a homogeneous, first-order function of its arguments, the third transform for a pure system is identically zero.[22,23]

Gibbs chose to base his development on the energy-explicit equation that is described by eq 1. At least one author before Gibbs (Massieu[27]) proposed the inverse (the entropy-explicit expression $S = f(U,V,N)$), but modern usage follows Gibbs, and only occasionally do we have a need for the alternate forms. An important situation where the entropy-explicit equation *is required* arises when a model of an *isolated* system is needed to fit Rudolph Clausius' statements of the first and second laws of thermodynamics[28] (for example, when developing criteria for equilibrium and stability). Callen[23] has discussed this topic in more detail.

The Legendre transform moves thermodynamic information among coordinate systems whose independent variables are related as slopes. Although the intensive variables temperature and pressure appear only as derivatives with the *USVN* function, they become coordinate variables for the transformed quantities, and thus the fundamental forms described by eqs 2, 3, and 4 are better suited to physical situations where those particular sets of independent variables are subject to control. However, such ideas for pure systems are well-understood and will not be pursued further here.

Before showing the pure-fluid models, it may be helpful to demonstrate graphically the effect of the Legendre transformation on the spatial geometry of a basic mathematical expression. To that end, we have chosen one that possesses features that are *qualitatively* similar to certain fundamental thermodynamic quantities. Consider as a base form

$$Z^{(0)} = k(1 - e^{-\alpha x_1}) + m{x_2}^3 \tag{5}$$

(Here, x_i is a general variable, not to be confused with its later usage as a chemical mole fraction.) The surface generated by eq 5 is shown in Figure 2a (for $m = 1$, $\alpha = k = 2$). The red region ($x_2 < 0$) is uniformly convex toward the viewer, but the green region ($x_2 > 0$) has a positive second derivative in the x_2-direction and is, thus, saddle-shaped. While the boundary between the two is a locus of inflection for this simple case, analogous features on thermodynamic surfaces—the stability-limit curves observed with specific transforms—do not coincide with a coordinate direction and appear skewed. Such curves are found on the surfaces generated by eqs 2 and 3 for pure fluids and also on those for certain higher-order binary and ternary transforms, as will be discussed later. In this paper, stability limits will always be designated by yellow−red boundaries.

To exercise the operation, let us take two first Legendre transforms and one second transform of the function described by eq 5 and observe the resulting geometries. We will indicate the procedure (following the notation of Model and Reid[22]), give the results, but omit the algebraic detail.

For

$$Z^{(k)} = f(x_1, x_2, \ldots, x_m)$$

$$Z^{(k)} = Z^{(0)} - \sum_{i=1}^{k} \left(\frac{\partial Z^{(0)}}{\partial x_i}\right) x_i$$

with

$$\left(\frac{\partial Z^{(0)}}{\partial x_i}\right)_{x_{j,j\neq i}} = \xi_i$$

$$Z^{(k)} = f(\xi_1, \ldots, \xi_k, x_{k+1}, \ldots, x_m) \tag{6}$$

Thus, based on eq 5,

$$Z^{(1)} = \frac{1}{\alpha}\left[\alpha k - \xi_1 + \xi_1 \ln\left(\frac{\xi_1}{\alpha k}\right)\right] + m{x_2}^3 \tag{7}$$

$$Z^{(1)} = \pm \frac{2{\xi_2}^{3/2}}{3\sqrt{3m}} + k(1 - e^{-\alpha x_1}) \tag{8}$$

$$Z^{(2)} = \frac{1}{\alpha}\left[\alpha k - \xi_1 + \xi_1 \ln\left(\frac{\xi_1}{\alpha k}\right)\right] \pm \frac{2{\xi_2}^{3/2}}{3\sqrt{3m}} \tag{9}$$

where $\xi_1 = \alpha k e^{-\alpha x_1}$ and $\xi_2 = 3m{x_2}^2$.

The transformed functions appear in Figures 2b, c, and d, with the new independent variables ξ_1 and ξ_2. Transforming in given directions results in new functions (here, $Z^{(1)}$ and $Z^{(2)}$), where one or both second derivatives have changed signs and the data have redistributed. Curves from the drawing in Figure 2a of constant x_1 (marked α, β, γ) and of constant x_2 (marked ρ, σ, τ) are labeled in their new positions on drawings 2b, c, d, as are the points corresponding to maximum and minimum values of x_1 and x_2.

The Legendre transform is not continuous through a point of inflection, and for the base equation 5, this results in a folding-back in the ξ_2-direction. The behavior here is the result of the $\pm$ term appearing in eqs 8 and 9 and is qualitatively similar to that observed with certain thermodynamic fundamental functions, for example, for pure systems when transforming from either the Helmholtz or enthalpy functions (eqs 2 and 3) to the Gibbs energy (eq 4).

Generalizing, the fold-back feature is observed with any (n + 1)th transform of an n-chemical-component, all-extensive

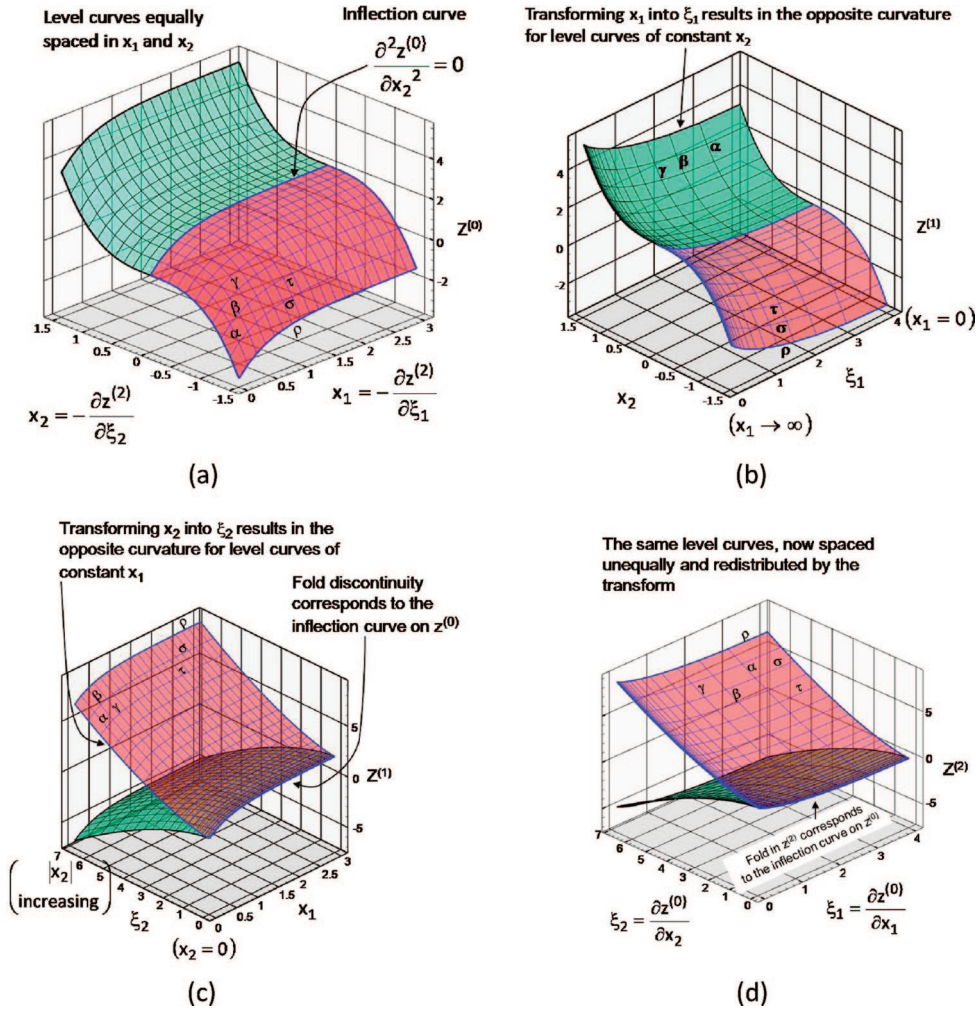

Figure 2. The function $Z^{(0)} = k(1 - e^{-\alpha x_1}) + m x_2^3$ and its Legendre transforms; $m = 1.0$, $\alpha = k = 2.0$.

Table 1. Material Properties[a]

No.	component	T_C (K)	P_C (bar)	ω	a	b ($\times 10^2$ K^{-1})	c ($\times 10^5$ K^{-2})	d ($\times 10^{10}$ K^{-3})
1	ethylene	282.4	50.36	0.086	0.4242	1.440	−0.4391	0
2	normal butane	425.16	37.97	0.201	0.9346	3.691	−1.140	0
3	carbon dioxide	304.15	73.76	0.231	1.675	0.7189	−0.4209	8.978

[a] Constant-volume, ideal-gas heat capacity is given as $C_V^0/R = a + bT + cT^2 + dT^3$, where temperature T is given in Kelvin. Interaction parameters for the mixture form of the Peng−Robinson equation are given as follows: $\delta_{12} = 0.0922$, $\delta_{13} = 0.0552$, and $\delta_{23} = 0.133$.

variable data set, or where all independent extensive variables except the final one have been replaced by their intensive conjugates. Such functions also are found in catastrophe theory and are called *swallowtails*.[29] We will see more examples of this behavior in the thermodynamic drawings that follow.

The role of eq 9 may now be reversed, so that it becomes the base function itself for back-Legendre transformation to recover eq 5 exactly, thus verifying that the procedure can be inverted and that the original information content has been retained throughout the process.

Thermodynamic Surfaces for Pure Fluids

We begin with the patriarch of all fundamentals, the all-extensive *USVN* function, constructed here for the vapor and liquid phases of ethylene (see Table 1). To obtain the 3-D variables for plotting, we scale with the number of moles and obtain the molar quantities U_N, S_N, and V_N. The surface is shown in Figure 3; this is the natural home for Gibbs' signature expression $d\varepsilon = t\, d\eta - p\, dv$. In all of the drawings shown here, the color blue denotes states that are absolutely stable and can be produced in the laboratory. Red regions represent unstable states—those whose very existence would violate the second law of thermodynamics through having no immunity to perturbation.[22,25] [One might argue that the red regions should not be shown, because states with those properties do not exist in nature. We show them to illustrate the contrasts in curvature between the globally stable blue and locally stable yellow regions, on one hand, and the always-unstable red regions on the other hand.] Yellow regions comprise the in-between or metastable states (here, these are superheated liquids or subcooled vapors). [We caution the inquisitive reader that superheated liquids can be dangerous. Reid[30] has discussed metastable liquids and referred to them as an "industrial curse".]

Because all drawings in this collection center around a vapor−liquid critical point (which is always indicated by a white cross), the variables that contain arbitrary constants (U_N, S_N, A_N, μ_i,...) are referenced to their critical values as well as made nondimensional. Thus, in Figure 3, $(U_N - U_{NC})/(RT_C)$ is the

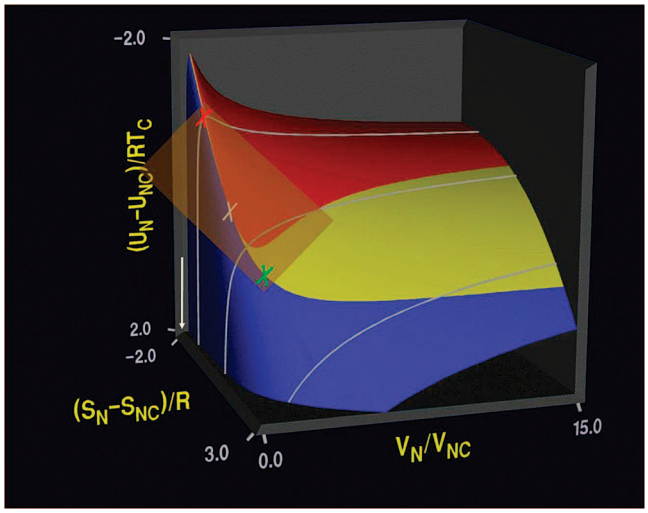

Figure 3. Energy−entropy−volume function for the fluid phases of ethylene: (red cross) = saturated liquid, and (green cross) = saturated vapor.

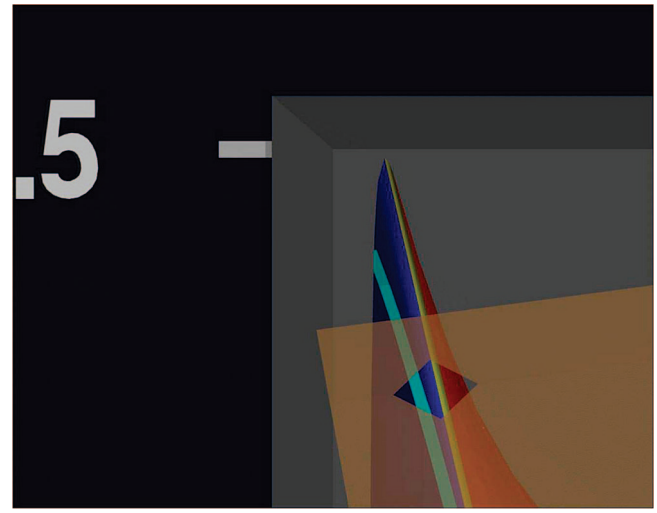

Figure 4. Enlargement of Figure 3, to show details of the liquid phase; the light blue line is a slightly subcritical isobar.

dimensionless difference between the molar energy at a general point and that at the critical point. Temperature and volume (and pressure, in subsequent figures) appear reduced in the usual ways. Note that energy is plotted positive-downward in Figure 3 and that the surface is crossed by three white curves of constant entropy.

The most revealing feature of the *USV* surface is its change from being uniformly convex outward (stable and metastable states) to being saddle-shaped (unstable states). The yellow-red boundary separates these regions and is, thus, the spinodal curve; however, in these coordinates, it is not determined by a single, vanishing, second derivative. For that, in a pure system, we must wait for the first transform.

Gibbs' "Rolling Plane"

In its unscaled, extensive form, $U = f(S,V,N)$ is four-dimensional and possesses three partial derivatives:

$$\left(\frac{\partial U}{\partial S}\right)_{V,N} = T \tag{10}$$

$$\left(\frac{\partial U}{\partial V}\right)_{S,N} = -P \tag{11}$$

$$\left(\frac{\partial U}{\partial N}\right)_{S,V} = \mu \tag{12}$$

While N-scaling for a pure fluid in a closed system seems natural, it denies us the opportunity to see the last of these partials in the same way that we see (and understand) the first two. However, it is a fortunate consequence of the spatial geometry of these models that the value of the *excluded slope* at any point (S, V, N) persists as the intercept on the axis through the origin of a plane tangent to the 3-D surface at the point (S_N, V_N). If a tangent plane were placed anywhere on the blue surface of Figure 3, with its convex nature, that tangency would be the sole contact point and we could obtain six numbers from it: the three spatial coordinates of the tangent point, U_N, S_N, and V_N; the two principal slopes, temperature T and pressure P (from eqs 10 and 11); and the value of the intercept of the plane on the axis through the origin (not shown here), which would be the chemical potential μ. However, for a pure fluid in a single phase, this is excess information. Recall that $N\mu = G = U - TS + PV$, so that knowing the slopes and the N-scaled coordinates gives μ directly.

However, if the position of tangency is as shown in Figure 3, where the plane straddles the red unstable region with its saddle surface, *two points* of tangency result, and, therefore, there are two remote points on the surface (i.e., with distinct values of U_N,S_N,V_N) that have the same principal slopes and that project via a common tangent to the same intercept on the axis through the origin. Therefore, the thermodynamic states represented by these two points may coexist in (phase) equilibrium, because they jointly satisfy the equilibrium criteria.

The dual tangencies in Figure 3 are marked with red and green crosses that denote, respectively, specific saturated liquid and vapor states of ethylene. The liquid point is difficult to see at the scale of the drawing, so the upper-left corner of the surface is enlarged in Figure 4 to show the details of the blue-yellow-red boundaries and the contact point of the plane (marked with a diamond cutout). The idea of *rolling* relates to the fact that as the tangent is rolled northeast (NE) from the critical point in Figure 3: its two contacts define the blue-yellow boundaries—successive pairs of points in vapor−liquid phase equilibrium—and, therefore, mark the two branches of the coexistence curve for ethylene in the energy−entropy−volume coordinates.

Gibbs described this clever method for locating phase-equilibrium states, and Maxwell responded by constructing the qualitative *USV* surface, shown in Figure 1. Maxwell's model supposedly represented the solid, liquid, and gaseous phases of water, so Gibbs' rolling scenario could be considered for *all three* common phase transitions: $L-V$, $L-S$, $S-V$. The models shown in this paper are based on a fluid-phase generating equation (the Peng−Robinson equation[19]), so only liquid−vapor coexistence can be illustrated in these computer drawings.

It is reassuring to note that, as the tangent plane rolls over the *USV* surface, its mechanical degrees of freedom match the variances given by the phase rule: two in the single-phase regions [the blue and (locally) yellow zones], one along any pair of coexistence curves (the blue-yellow boundaries), and zero at the unique, three-point tangency that occurs at the triple point [realizable with both Maxwell's surface and also with the model by Clark and Katz (see Figure 1)]. For more details the reader is referred to Gibbs' second paper[7] and also to Figure 5.2b in ref 31.

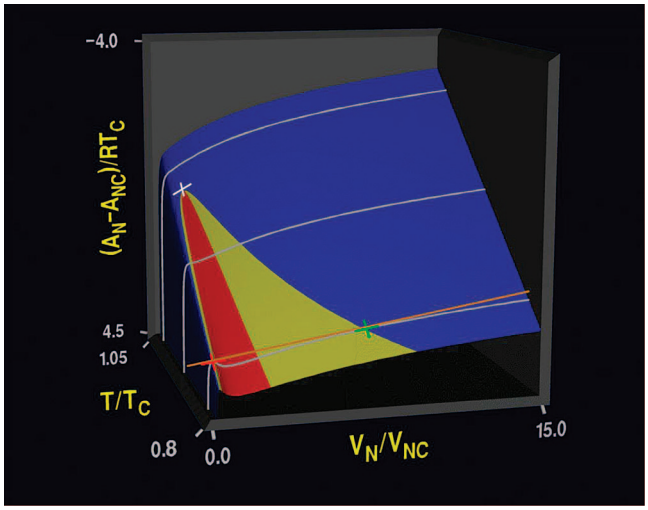

Figure 5. The Helmholtz energy.

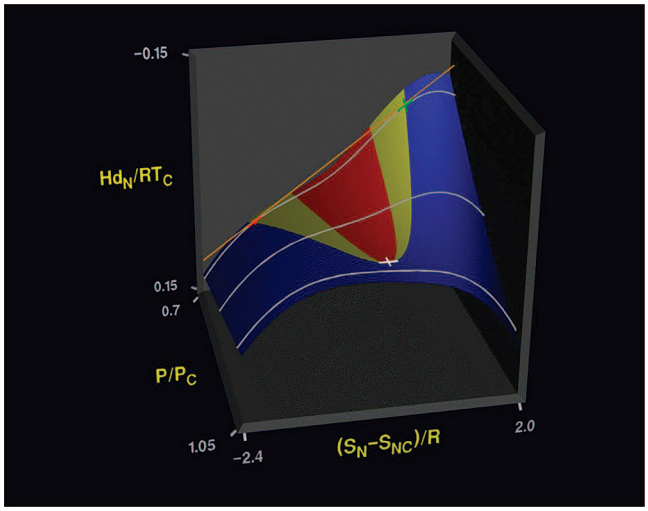

Figure 6. The enthalpy (differenced).

We will see the rolling plane again in two later examples involving mixtures.

Transformed Functions

The first-transform surfaces produced by the operations described in eqs 2 and 3 are shown scaled in Figures 5 and 6, with the dependent variables again plotted positive-downward. In both cases, the yellow-red spinodal loci have become inflection curves, defined by the compact stability-limit expressions

$$\left(\frac{\partial^2 A_N}{\partial V_N^{\,2}}\right)_T = 0 \tag{13a}$$

$$\left(\frac{\partial^2 H_N}{\partial S_N^{\,2}}\right)_P = 0 \tag{13b}$$

The changes in curvature between the yellow and red regions are slight but can be seen by looking at the near edge of the Helmholtz surface and at the far edge of the enthalpy diagram. The tangent structures drawn are now single brown lines that represent a specific reduced temperature in Figure 5 and a specific reduced pressure in Figure 6. Each line straddles the unstable region and is tangent to a saturated liquid state (red cross) and a saturated vapor (green cross) on the blue-yellow boundaries. The Helmholtz tangent is for a reduced temperature T_r with a value somewhat greater than 0.8 and has a slope equal to the negative value of the dimensionless vapor pressure at that temperature: $-V_c P_{sat}(T)/(RT_c)$.

While the natural Helmholtz energy has sufficient surface variation at $T_r = 0.8$ for these effects to be visible, the natural enthalpy function does not. If the enthalpy surface were drawn using the same relative plotting scale as with the Helmholtz energy, it would appear flat. To make its variation visible, we must magnify it. This is done in Figure 6 by plotting the dimensionless difference between the molar enthalpy calculated at a general point (S_N,P) and a reference enthalpy taken at the same (S_N,P) values but from a plane tangent to the surface at the critical point. The differenced quantity plotted is called $Hd_N/(RT_C)$, and it magnifies the vertical variable by a factor of ~20. Thus, the curvature change across the yellow-red boundary is visible in Figure 6, and the isobaric tangent line is seen to straddle the unstable region in the same way as that previously observed and contact the coexisting $L-V$ states on either side (liquid to the left, vapor to the right). Although the slope of the *differenced* function changes sign in Figure 6, the natural enthalpy has a uniformly positive slope with entropy, as it must:

$$\left(\frac{\partial H_N}{\partial S_N}\right)_P = T > 0 \tag{14}$$

By analogy with the *USV* example, the *excluded* chemical potential persists also in Figures 5 and 6 as intercepts of the isothermal (isobaric) tangent lines on the vertical axes at $V(S) = 0$. As previously stated, this confirms that all pairs of states having a *common* tangent, again satisfy the three criteria for phase equilibrium in a pure fluid. A more-detailed, two-dimensional drawing of the Helmholtz scenario may be seen in refs 31 (p 216) and 32.

Figure 7a shows the final pure-fluid fundamental, the doubly transformed swallowtail function produced by the operation described by eq 4, the Gibbs energy. With both independent variables now intensive and the dependent variable G_N identical to the chemical potential, coexisting phases in these coordinates are designated by a single curve of points common to both. Thus, the surfaces for the vapor phase (low pressure) and for the liquid phase (high pressure) intersect in a single coexistence curve and continue through it to form the metastable regions: transparent yellow sheets in Figure 7a that represent superheated liquid to the left, subcooled vapor to the right. Because the Gibbs energy is an $(n + 1)$ transform for pure ethylene, fold-back behavior occurs from both metastable branches to form the unstable region, which comprises a cap covering the metastable states and the coexistence curve. We omit it here because it would block the view, but imply it with several folded-back red lines. [Fold-back behavior in Figure 7a can be understood from either Figure 5 or from the detailed Helmholtz drawing in refs 31 (p 216) and 32. Moving along any isothermal path at $T < T_c$, both the slope P and the intercept G (or μ) of the tangent reverse direction as the volume enters the unstable zone from either metastable zone surrounding it.] The complete 3-D swallowtail, *containing* the unstable region, may be seen in ref 12 (p 320). Several authors have shown typical isothermal traces, $G = f(P)_T$.[23,25,33]

A vertical line drawn in Figure 7a at values of T_r and P_r not far from the coexistence curve would pierce all three branches of the Gibbs energy surface (blue, yellow, red). This observation

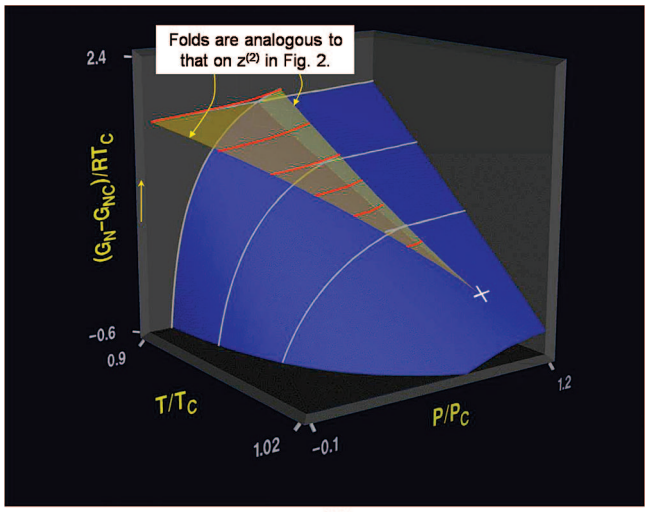

(a)

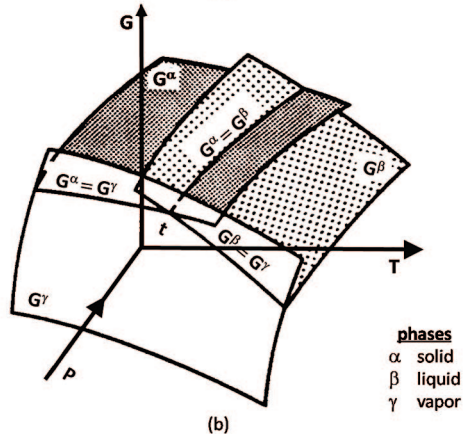

(b)

Figure 7. (a) Gibbs energy (fluid phases only), and (b) Gibbs energy for the three common phases (t = triple point). (Figure 7b reprinted with permission from ref 34. Copyright C. H. P. Lupis.)

visually confirms the well-known fact that G is at a minimum for the most-stable state among any group of states constrained at (T,P,N).

The drawing depicted in Figure 7b, from the work of Lupis,[34] is a sketch of the Gibbs energy for the combination of the solid, liquid, and vapor phases. It shows the invariant triple point t and (conceptually) the overlapping metastable zones. The line marked $G^{\beta} = G^{\gamma}$ is the $V-L$ coexistence curve and corresponds to the intersection of the blue vapor and liquid regions in Figure 7a.

We have shown three types of surface geometry that enable coexisting, phase-equilibrium states to be visualized by observing, respectively, a tangent plane, a tangent line, and points along the self-intersection of surface segments. These geometries persist as we increase the order of the system from pure to binary to ternary, etc., and the transform level yielding a given geometry advances with each additional chemical component. Thus, first-transform surfaces in a binary system may be treated with Gibbs' rolling plane, and fourth-transform surfaces for a ternary show self-intersecting, swallowtail behavior. We shall see these cases in the sections on mixtures.

Equations of State: Derivative Functions

We follow the language of Callen[23] and Model and Reid[22] by referring to any first derivative of any fundamental form as an equation of state (EOS). As noted earlier, for the special cases where all EOS variables are measurable, one uses the more-restrictive term, *phase diagram*.

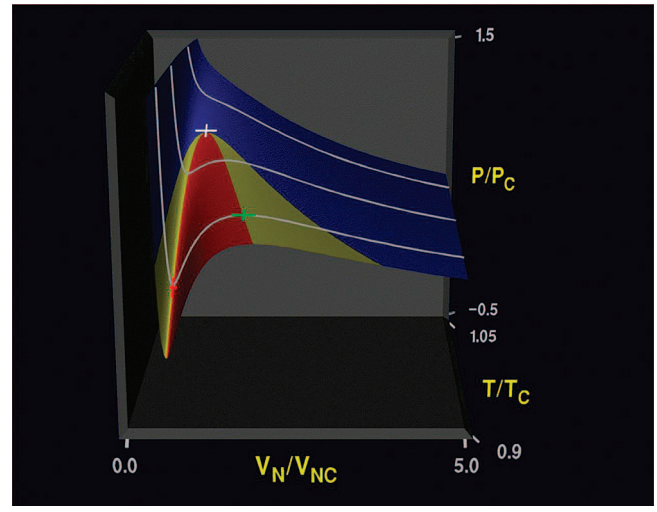

Figure 8. *PVT* function from the Peng−Robinson equation.[19]

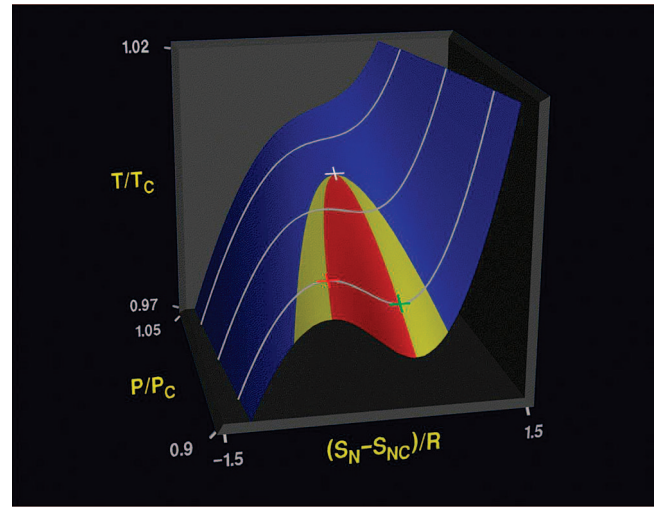

Figure 9. Temperature−entropy−pressure diagram.

Two EOS examples are shown for pure fluids: the familiar *workhorse* PV_NT function, obtained formally by differentiation of the Helmholtz energy, with respect to volume, and the TS_NP function, which is obtained from the enthalpy via differentiation with respect to entropy. For this collection, Figure 8 is simply a plot of the cubic Peng−Robinson equation with the metastable and unstable regions exposed. What were points of inflection for the Helmholtz function are now extrema on the PV_NT phase diagram. The two subcritical isotherms in Figure 8 show the minimum/maximum behavior that is typical of any cubic curve, and the colored crosses now indicate the spinodal points.

The TS_NP function drawn in Figure 9 is the three-dimensional counterpart of the familiar T-S diagram, which is another workhorse of engineering thermodynamics, particularly for the design of power cycles. Figures 9 and 6 are related in the same way as Figures 8 and 6 are related.

The TS_NP surface for water and steam, showing the ruled two-phase region instead of the metastable and unstable zones, was an early product of the computer graphics research in this laboratory. It appeared *colorized* on the dust jacket of the thermodynamics textbook by Smith, Van Ness, and Abbott (fifth edition)[35] and was shown even earlier by Sears as a line drawing (see ref 15, p 158).

Equation-of-state functions derived from cubic-equation-based property predictions form *cusp catastrophes*.[36]

Diagrams for Mixtures

In his famous monograph, *Molecular Thermodynamics of Fluid-Phase Equilibria*,[37] John Prausnitz wrote that "We live in a world of mixtures...". While no rigorous development of the macroscopic thermodynamics of equilibrium (MTE)[38] could proceed without the introduction provided by the pure-fluid basics, engineers must move through that and go on to the more chemically interesting, industrially important, and, for this paper, dimensionally complex examples involving two or more components. Here, we will consider one binary and one ternary combination. While the explanations of the drawings will be more complicated, we will be relieved to find that the *regularity* of the Gibbs models helps organize our thinking and once again affirms the universality of thermodynamic analysis.

We consider two types of independent-variable sets: symmetric and asymmetric.

1. Symmetric.

$$\text{extensive notation:} \quad U = f(S,V,N_1,N_2,...,N_n)$$

$$\text{conjugate intensive variables:} \quad T,P,\mu_1,\mu_2,...,\mu_n$$

with

$$\mu_i = \left(\frac{\partial U}{\partial N_i}\right)_{S,V,N_{j,j\neq i}}$$

Dividing by N_n scales the variables, to yield mole-number-based quantities (S/N_n, H/N_n,...) and mole-ratio compositions ($0 \leq N_i/N_n < \infty$)

Legendre transforms taken with respect to symmetric mole numbers are indicated by one or more prime symbols and yield conventional chemical potentials. For example, for the third transform in a binary system, conventional ordering:

$$\text{base function:} \quad U = f(S,V,N_1,N_2)$$

$$\text{third transform, unscaled:} \quad G' = U - TS + PV - \mu_1 N_1 = f(T,P,\mu_1,N_2) \quad \text{(5-dimensional)}$$

$$\text{scaled:} \quad \frac{G'}{N_2} = f(T,P,\mu_1) \quad \text{(4-dimensional)}$$

$$\text{at a fixed temperature:} \quad \left(\frac{G'}{N_2}\right)_T = f(P,\mu_1)_T \quad \text{(3-dimensional)}$$

2. Asymmetric.

$$\text{extensive notation:} \quad U = f(S, V, N_1, N_2, \ldots, N_{n-1}, N)$$

$$N = \sum_1^n N_i$$

$$\text{conjugate intensives:} \quad T,P,\eta_1,\eta_2,...,\eta_{n-1},\eta_n$$

η is a modified chemical potential: $\eta_i = \left(\frac{\partial U}{\partial N_i}\right)_{S,V,N_{j,j\neq i,n},N} = \mu_i - \mu_n \quad (\eta_n = \mu_n)$

Equality of η_i between phases guarantees equality of μ_i, thus assuring chemical equilibrium. [Conventional chemical potentials μ_i remain finite as $x_i = N_i/N \rightarrow 1.0$ but become negatively infinite as $x_i \rightarrow 0$. The modified chemical potentials η_i are unbounded at both concentration extremes.]

Dividing by N scales the asymmetric variable set, to yield molar quantities (S_N, H_N,...) and mole-fraction compositions ($0 \leq N_i/N = x_i \leq 1.0$).

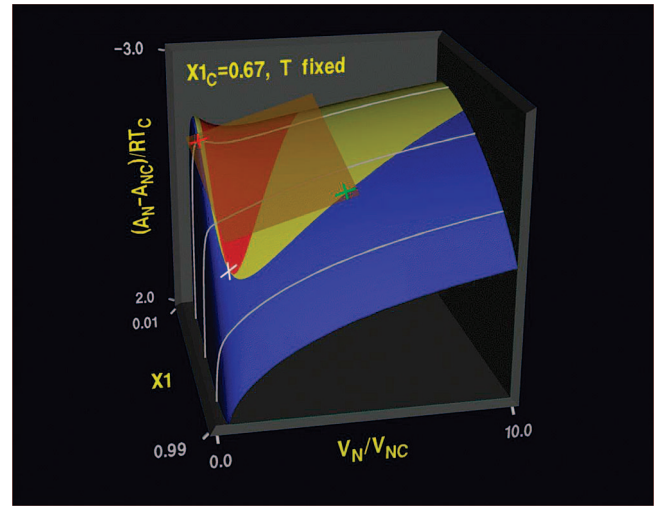

Figure 10. Helmholtz energy for the ethylene (1)−normal butane (2) system at 347 K.

Legendre transforms taken with respect to asymmetric mole numbers are indicated by one or more plus signs and yield modified chemical potentials. For example, for the third transform in a ternary system, conventional ordering:

$$\text{base function:} \quad U = f(S,V,N_1,N_2,N)$$

$$\text{third transform, unscaled:} \quad G^+ = U - TS + PV - \eta_1 N_1 = f(T,P,\eta_1,N_2,N) \quad \text{(6-dimensional)}$$

$$\text{scaled:} \quad \frac{G^+}{N} = f(T,P,\eta_1,x_2) \quad \text{(5-dimensional)}$$

$$\text{at fixed temperature and pressure:} \quad \left(\frac{G^+}{N}\right)_{T,P} = f(\eta_1,x_2)_{T,P} \quad \text{(3-dimensional)}$$

Drawings for Binary Systems

The model system is ethylene (1)−normal butane (2) (again, see Table 1, "Material Properties"). We begin with a first Legendre transform, conventional ordering, asymmetric variable set, and show the surface in Figure 10. This is the Helmholtz energy for the binary, restricted to a single temperature (347 K) such that the composition of the critical point is $x_{C(ethylene)} = 0.67$ and the critical pressure is 67.9 bar. Following the symbolism already given, the function in dimensional terms is

$$A_N = f(V_N,x_1)_T$$

After being referenced to the critical point and nondimensionalized as in the earlier figures, it becomes

$$\frac{A_N - A_{NC}}{RT_C} = f\left(\frac{V_N}{V_{NC}}, x_1\right)_T$$

The function is plotted positive-downward, to make the blue-yellow regions convex toward the viewer and place the tangent plane on the viewer's side of the surface. The geometry of this binary first transform is the same as that of the base function (*USV*) for pure fluids, and it is drawn in Figure 10 with a transparent tangent. The plane straddles the red unstable region and has rolled NE from the critical point, its two contacts tracing the blue-yellow boundaries and its slope in the volume direction -P decreasing steadily. The plane is resting at a saturated liquid point, 16% C_2H_4 (red cross), and at a saturated vapor point, 59% C_2H_4 (green cross), which constitute jointly an equilibrium

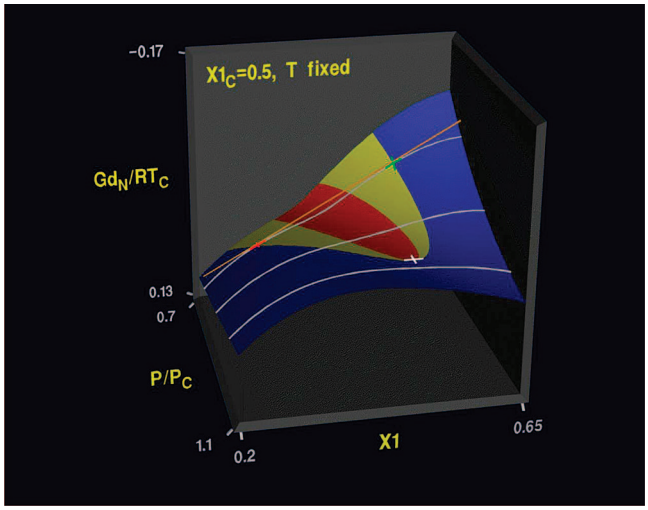

Figure 11. Binary Gibbs energy (differenced) at 375 K.

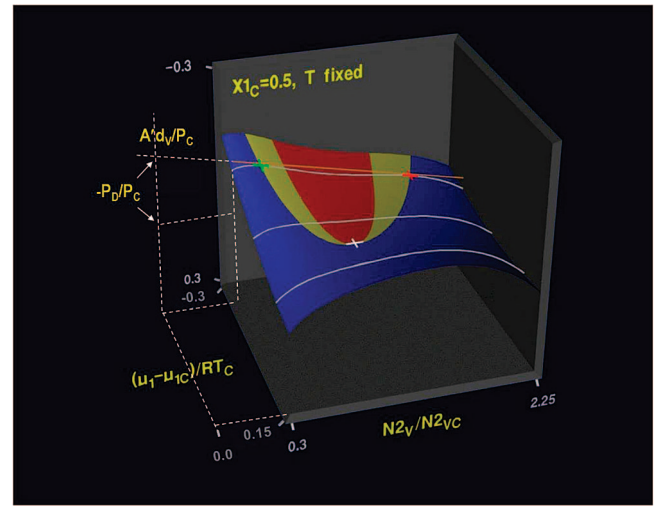

Figure 12. Visualization of eq 16, the modified Helmholtz energy A' (volume-scaled and differenced), a second Legendre transform.

pair according to the following:

(I) The points are part of an isothermal surface and, therefore, are at the same temperature (347 K).

(II) Both points are contacted by the same tangent plane and are thus at the same pressure P (negative slope in the volume direction, here 25.8 bar) and have the same modified ethylene chemical potential η_1 (slope in the x_1 direction). [$\eta_i = (\partial A/\partial N_i)_{T,V,N_{j,j}}$; scaling with N gives $\eta_i = (\partial A_N/\partial x_i)_{T,V_{N,xj}}$; for a binary system, $\eta_1 = (\partial A_N/\partial x_i)$.]

(III) They both project (via the plane) to the same intercept on the vertical axis through the origin ($x_1 = 0$, $V_N = 0$) and therefore have the same butane chemical potential η_2. [Numerical values are not given for η_1 or η_2, because they have no physical meaning. Chemical potential contains arbitrary constants.]

As with USV for a pure material, the change from metastable to unstable corresponds to a change in surface character from locally convex (yellow) to saddle (red). But again, in these coordinates, that transition cannot be represented by a single, vanishing, second derivative.

We show two binary second transforms. The first is the familiar isothermal Gibbs energy, differenced and plotted positive-downward in Figure 11 against reduced pressure and ethylene mole fraction, for the temperature (375 K) that yields the equimolar critical point.

$$\text{extensive (asymmetric) form:} \quad G = f(T,P,N_1,N)$$

$$\text{differenced and scaled:} \quad (Gd_N)_T = f(P,x_1)_T$$

One supercritical and two subcritical isobars cross the surface in Figure 11. The lowest of the three (at a reduced pressure of $P_r \approx 0.75$) is accompanied by a tangent line denoting saturated, equilibrium states on the opposing blue-yellow boundaries. The four phase-equilibrium criteria are satisfied in a manner analogous to those for the previous case.

The second example is the primed (or modified) Helmholtz energy, written here in extensive, symmetric variables—a five-dimensional form:

$$A' = U - TS - \mu_1 N_1 = \mu_2 N_2 - PV = f(T,\mu_1,N_2,V) \qquad (15)$$

[There are no common names for transforms taken with respect to mole numbers.] When the temperature is fixed as observed previously (375 K), and the function is differenced and volume-scaled, one obtains the three-dimensional version that is plotted in Figure 12:

$$(A' d_V)_T = f(\mu_1,N_{2V}) \qquad (16)$$

The chemical potential is referenced to its critical value in the same way as the previous dependent variables. N_{2V} (or N_2/V) is the molar density of component 2 (normal butane), and the critical point is the same physical state as in the previous drawing.

Volume-scaling excludes the *pressure* from direct display in 3-D sections of higher-dimensional thermodynamic functions. However, by analogy with the earlier examples of N-scaling, the pressure at any point may still be observed from the intercept of the appropriate line or plane tangent to the surface at that point. The brown tangent line of fixed μ_1 in Figure 12 has been extended (dashed) to its intersection with the dashed vertical axis at $N_{2V} = 0$. This gives the dimensionless, differenced pressure ($-P_d/P_c$) that corresponds to the equilibrium liquid and vapor states shown by the red and green crosses.

As noted previously, each of the special coordinate systems of MTE conforms to a physicochemical system constrained in a particular way. Figure 13 shows an experimental arrangement that corresponds to the A' function just defined. [Figure 13 was created by William Beach, graphic designer in the College of Engineering at Iowa State University. It acknowledges and applauds the collection of wryly humorous illustrations in the textbook by Model and Reid[22] (now Model and Tester[31]). Those drawings were created by MIT chemical engineering graduate student Tetsuo Maejima, with important contributions from the late Professor Robert C. Reid.] The source of species 1 holds μ_1 constant through a semipermeable membrane while species 2 is being added to the cell. Such an apparatus might be used with single phases for determining the dependence of pressure on composition or the dependence of chemical potential on volume.

$$\left(\frac{\partial P}{\partial N_2}\right)_{T,\mu_1,V} = -\left(\frac{\partial^2 A'}{\partial V\,\partial N_2}\right) = -\left(\frac{\partial \mu_2}{\partial V}\right)_{T,\mu_1,N_2}$$

It might be used also to demonstrate the phase-change behavior shown in Figure 12 along the blue-yellow boundaries.

Recall that experiments in thermodynamics are performed with fully extensive, not scaled, quantities. The reduction to molar variables and to mole-fraction compositions is most often

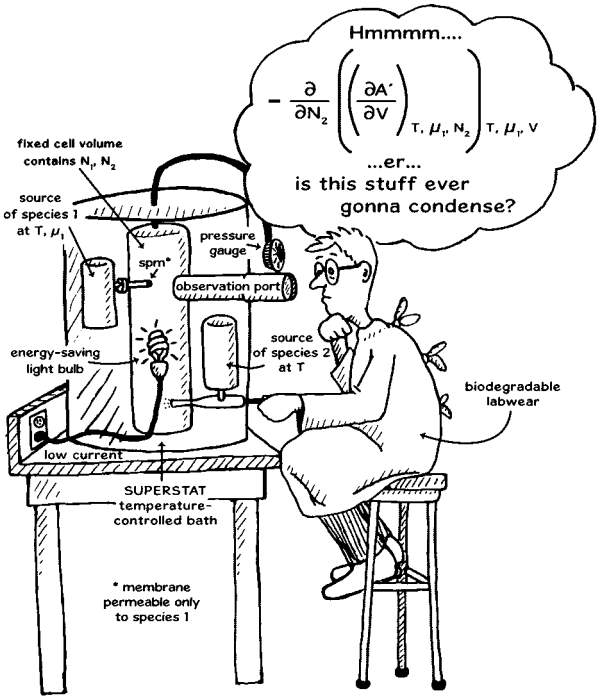

Figure 13. Experimental cell for studying eq 16. (Illustration provided by William Beach, Iowa State University, 2008.)

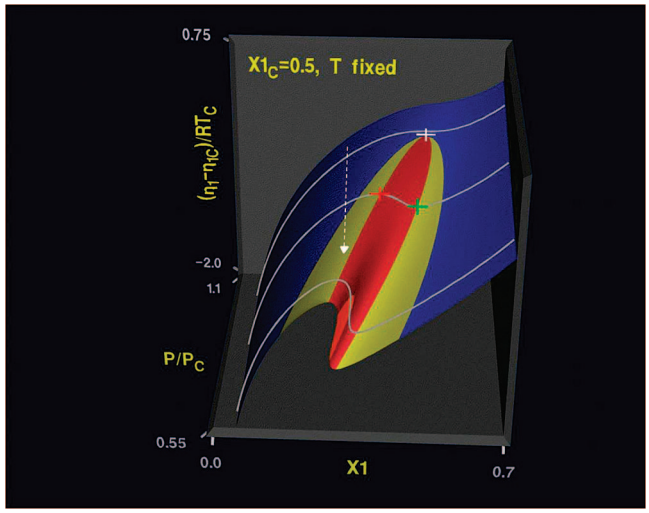

Figure 14. Binary equation-of-state (EOS) function, $\eta_1 = f(P, x_1)_T$.

done for convenience and to allow for the compact display of data. Thus, these results could be plotted also as

$$\frac{Ad_V^+}{P_c} = f(\eta_1, N_V)_T$$

where N_V is the total molar density.

For both of the previous second transforms, the yellow-red stability limits (spinodals) are curves of inflection, which can indeed be represented by single, vanishing, second derivatives:

$$\left(\frac{\partial^2 G_N}{\partial x_1^2}\right)_{T,P} = 0 \quad \left(\frac{\partial^2 A'_V}{\partial (N_{2V})^2}\right)_{T,\mu_1} = 0 \tag{17}$$

A Binary Equation of State

We show a single EOS for ethylene−normal butane derived from the Gibbs energy function displayed in Figure 11. Using extensive variables:

$$\left(\frac{\partial G}{\partial N_1}\right)_{T,P,N} = \eta_1 = f(T, P, N_1, N)$$

Scaling by N and fixing the temperature at 375 K yields $\eta_1 = f(P,x_1)_T$. Figure 14 shows the EOS function, referenced to its critical value and made nondimensional.

$$\frac{\eta_1 - \eta_{1C}}{RT_C} = f\left(\frac{P}{P_c}, x_1\right)_T$$

The inflection curves of the Gibbs energy again produce minima and maxima on this surface, as highlighted by the crosses on the center white isobar. Over most of the red region ($0.65 < P_r < 1.0$), the slope in the composition direction is negative:

$$\left(\frac{\partial \eta_1}{\partial x_1}\right)_{T,P} < 0$$

This violates the first diffusional stability criterion, and no real state of the mixture can exhibit such behavior.

Multicomponent systems possess a hierarchy of stability limits, with each additional component adding a more restrictive condition and causing the true limit to be reached sooner than would be expected from the lesser restrictions.[22,25] For the pure systems previously discussed, two criteria were in effect for stable and metastable states:

(1) For thermal stability (conventional ordering):

$$\left(\frac{\partial^2 U}{\partial S^2}\right)_{V,N} = \frac{T}{NC_V} > 0 \tag{18}$$

(2) For mechanical stability (implied earlier by eq 13a):

$$\left(\frac{\partial^2 A}{\partial V^2}\right)_{T,N} = -\left(\frac{\partial P}{\partial V}\right)_{T,N} > 0 \tag{19}$$

The latter condition was controlling for the pure cases and thus dictated the properties along the yellow−red boundaries in Figures 3–9. The presence of a second component now imposes a third, yet-more-restrictive condition on binary mixtures. This is called the first-diffusional criterion, and, with conventional ordering of asymmetric variables, it becomes

$$\left(\frac{\partial^2 G}{\partial N_1^2}\right)_{T,P,N} = \left(\frac{\partial \eta_1}{\partial x_1}\right)_{T,P} > 0 \tag{20}$$

For $P_r < 0.65$, an orange region within the red zone develops in Figure 14, where the surface first becomes vertical and then tilts back at still lower pressures to show a positive slope over a small composition range. This is barely visible on the lowest white isobar ($P_r \approx 0.6$) but is more pronounced along the near edge of the orange region itself. This behavior is an artifact of how the various stability limits (thermal, mechanical, first-diffusional,...) relate to each other. The latter two are linked as follows:[22]

$$\left(\frac{\partial^2 G}{\partial N_1^2}\right)_{T,P,N} = \frac{\begin{vmatrix} \left(\frac{\partial^2 A}{\partial V^2}\right)_{T,N} & \left(\frac{\partial^2 A}{\partial V\,\partial N_1}\right) \\ \left(\frac{\partial^2 A}{\partial V\,\partial N_1}\right) & \left(\frac{\partial^2 A}{\partial N_1^2}\right)_{T,V,N} \end{vmatrix}}{\left(\frac{\partial^2 A}{\partial V^2}\right)_{T,N}} = \left(\frac{\partial^2 A}{\partial N_1^2}\right)_{T,V,N} - \frac{\left(\frac{\partial^2 A}{\partial V\,\partial N_1}\right)^2}{\left(\frac{\partial^2 A}{\partial V^2}\right)_{T,N}} \tag{21}$$

The left side of eq 21 (the first diffusional criterion, term a) relates directly to the surfaces in Figures 11 and 14, but the terms on the right are more readily associated with Figure 10, which is the binary Helmholtz function. Two of the three derivatives on the right are directly visible from slope variations in Figure 10, and the mechanical stability criterion (eq 19; here, term b) appears in the denominator. At any (locally) stable (blue-yellow) state in Figure 14, terms a and b must both be positive. Moving from that point toward the yellow-red spinodal causes term a (and, thus, also the right side of eq 21) to reach zero before term b and the isobar to show a zero slope accordingly. Crossing into the unstable region at $P_r > 0.65$ results in a negative slope, but continued movement toward the opposite spinodal reverses that change, and the slope returns to zero and then to a positive value again in the opposite metastable zone. For $P_r > 0.65$, term b remains positive and has no influence on the *sign* of the slope.

For $P_r < 0.65$, within the red zone, term b also becomes negative and the isobar develops a positive slope, which then defines the orange region. Term b is the mechanical stability criterion and was controlling in the pure-fluid cases. Here, it has the same mathematical role but is being used with a mixture whose composition changes along any isobar.

That complication is avoided if a constant-composition path is followed into and out of the unstable region, as begun by the dashed white line in Figure 14. Now the terms in eq 21 are applied to a fluid of fixed temperature and composition, where only pressure and volume change along the path. Again, the diffusional limit is violated first, and, for the same reasons, but one might now say that the subsequent *inner* violation (entering the orange zone) corresponds to crossing the mechanical limit of a *pseudo-pure* fluid with *PVT* properties identical to those of the fixed-composition, single-phase binary. Such an example, for a mixture of ethane and normal butane, is worked numerically in chapter 9 of ref 22

Drawings for Ternary Systems

For a ternary mixture, we add carbon dioxide (3) to the ethylene (1)−normal butane (2) binary previously modeled. We show three fundamental forms: the second, third, and fourth Legendre transforms. The geometries of these surfaces coincide with the three fundamental geometries already noted, where a tangent plane, a tangent line, or self-intersection defines coexisting phases in regions of metastable and unstable liquid−vapor states.

The critical locus of this ternary yields an equimolar critical point at 350 K and 7.53 MPa. With three components,we must now fix two quantities to have surfaces that can be plotted in three dimensions.

The first example is the Gibbs energy−composition diagram for the system. Asymmetric variables and *N*-scaling give

$$\frac{G}{N} = f(T, P, x_1, x_2)$$

Differencing, fixing the temperature and pressure as noted previously, and nondimensionalizing yields the function that is depicted in Figure 15.

$$\frac{Gd_N}{RT_C} = f(x_1, x_2)_{T,P}$$

As the order of the mixture increases, it becomes increasingly difficult to place the variable ranges considered in these drawings in context with the global property diagrams of the systems that they represent. Therefore, it may be helpful to

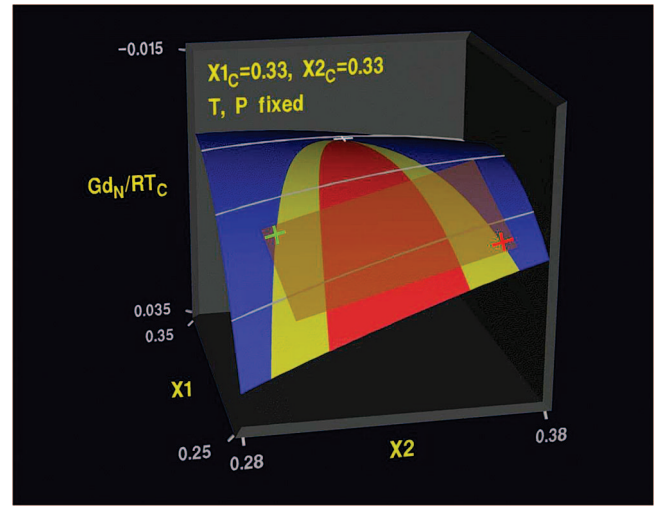

Figure 15. Gibbs energy for the ternary system involving ethylene (1), normal butane (2), and carbon dioxide (3). Conditions: $T = 350$ K, $P = 7.53$ MPa.

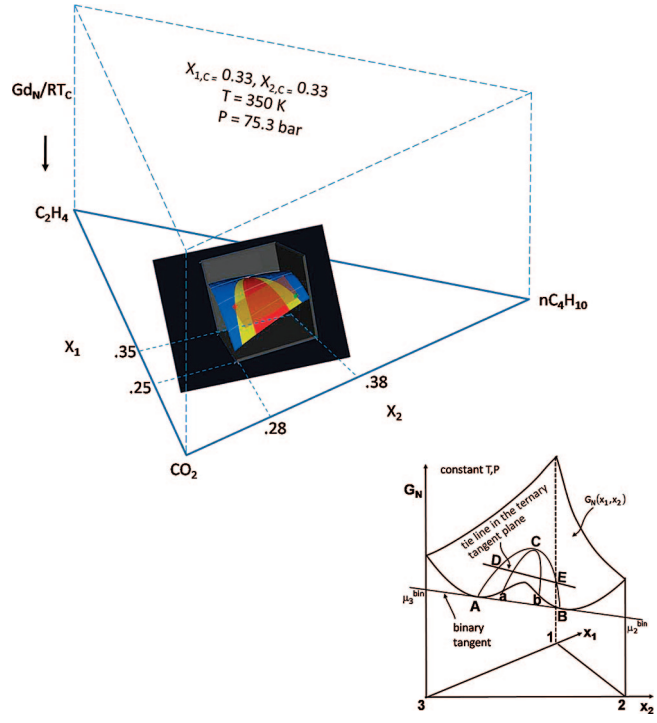

Figure 16. Placement of the Gd_N plot (shown in Figure 15) in ternary phase space. (Inset adapted from Prigogine and Defay.[39])

view the small composition rectangle shown in Figure 15 relative to the complete right prism that one would use for full display of the ternary Gibbs energy function. This is attempted in Figure 16.

As a second transform for a ternary mixture, the Gd_N geometry is analogous to that of the Helmholtz energy in Figure 10 and the *USV* base function in Figure 3. With Gd_N drawn positive-downward, the tangent plane is on the viewer's side of the surface, and it has rolled from the critical point (white cross) toward the viewer, tracing the blue−yellow boundaries (the coexistence curves) and stopping at the red/green states that have the compositions shown in Table 2.

In addition to being at the same temperature and pressure, these states are guaranteed to be in equilibrium, because they are both fit tangent to a single plane which, if extended, would

Table 2. Ternary VLE Compositions (at $T = 350$ K, $P = 7.53$ MPa)

No.	Composition (mole fraction) component	liquid (red)	vapor (green)
1	ethylene	0.27	0.30
2	normal butane	0.37	0.30
3	carbon dioxide	0.36	0.40

yield intercepts on the pure-component axes of the prism (see Figure 16), giving both states common values of

$$\overline{G_i} = \left(\frac{\partial G}{\partial N_i}\right)_{T,P,N_{j,j\neq i}} = \mu_i$$

for each component. $\bar{G}_i$ is the partial molar Gibbs energy.

The blue and yellow regions of Figure 15 are convex, and the red region is again saddle-shaped. However, even with differencing, the contour changes are so slight that they are barely visible, even along the near edge of the drawing, where $x_1 = x_{eth} = 0.25$. If the Gd_N function were continued toward $x_1 = 0$, the changes would become more pronounced and the various regions of the surface would intersect the $CO_2-nC_4H_{10}$ face of the prism in a typical, isothermal−isobaric, binary $G-x$ curve, with coexisting $L-V$ states at $x_{2,liq} \approx 0.43$ and $x_{2,vap} \approx 0.26$. The inset in Figure 16, adapted from Prigogine and Defay,[39] shows exactly that scenario, with points A and B designating the binary $V-L$ states and points D and E designating the ternary states, analogous to the green and red crosses on the main drawing. Gibbs energy is plotted positive-upward in the inset, which explains the opposite convexity. [A drawing analogous to the Prigogine sketch in Figure 16, but following the metastable−unstable regions for a *binary* mixture moving toward one of its *pure components,* appears in Dr. Coy's dissertation.[20] His Figure IV.38 traces the spinodal and coexistence curves through (GPx) space, from the 375 K critical point of Figure 11 (this paper), over the undifferenced, isothermal Gibbs energy surface, and ending at the edge of the function ($x_1 = 0$), where they terminate in the $G_N = f(P)_T$ curve for normal butane.]

Carbon dioxide and ethylene form a minimum-boiling azeotrope, but at conditions far removed from those considered here for the mixture with normal butane in the critical region. There is no influence of that behavior on the equilibria shown in Figure 15, and it is interesting to note that the presence of normal butane in natural gas actually makes it useful as a separating agent for the azeotropic binary.[40]

Figure 17 shows a third transform for the ternary in asymmetric variables, with temperature and the modified chemical potential of normal butane (η_2) fixed, again to yield the equimolar critical point. Differencing and molar scaling give

$$A^{++}d_N = f(\eta_1, V_N)_{T,\eta_2}$$

By analogy with Figure 12, the value of η_3 ($= \mu_3$ (or μ_{CO_2})) common to any equilibrium liquid and vapor pair is obtained from the intercept of the common tangent line at $V_N = 0$, and the pressure is related (through the differencing) to its slope. Because η is a contrived measure of chemical potential, its value cannot be held constant using a single control device. To fix η_2 as indicated, one must fix the *difference* between μ_2 and μ_3, using appropriate chemical sources analogous to those sketched in Figure 13. Therefore, with the temperature also fixed, the phase rule allows two additional free independent variables to specify the state of the ternary in a single phase. Pressure and total molar volume comprise one pair of choices, which would then set the value of η_1 and, thus, μ_1. Another pair would be the pressure and the amount of ethylene N_1 in the fixed volume, which would then determine the total molar volume and all dependent quantities.

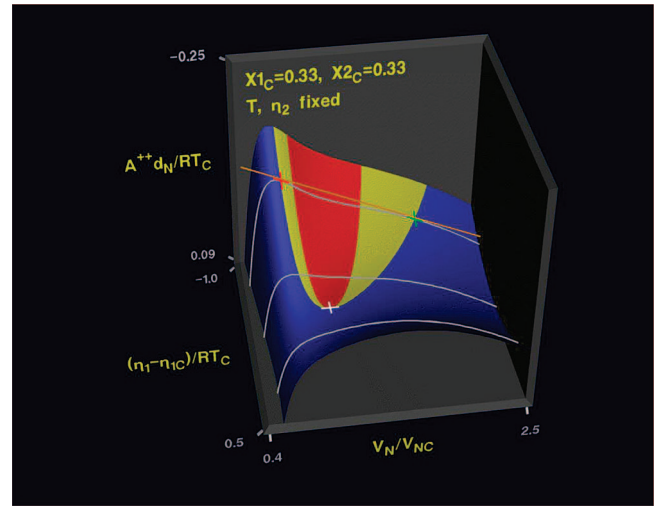

Figure 17. The ternary A^{++} function.

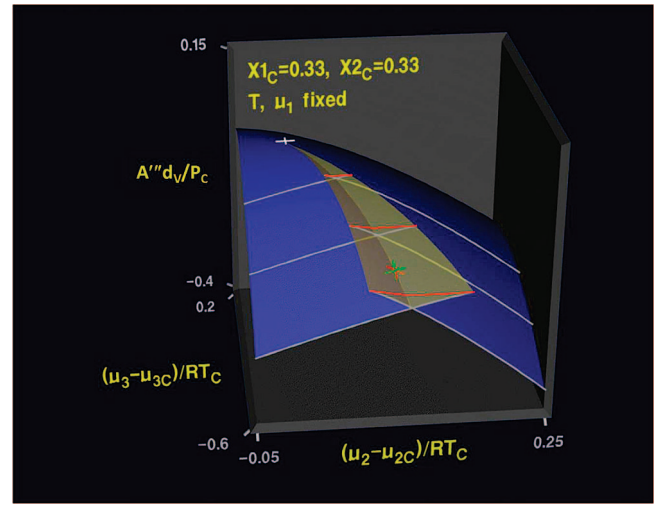

Figure 18. The fourth transform, swallowtail, $A^{'''}$ surface, from eq 22.

As with any ternary third transform, the spinodal loci in Figure 17 are inflection curves that are designated by

$$\left(\frac{\partial^2 A^{++}}{\partial V^2}\right)_{T,\eta_1,\eta_2,N} = -\left(\frac{\partial P}{\partial V}\right)_{T,\eta_1,\eta_2,N} = 0$$

Although these compact expressions are correct formally, they contain the nonmeasurable quantities A^{++} and η_i. To determine the *physical conditions* along the stability-limit curves, we must re-express the derivatives in terms of measurable variables only. This is done most often by *stepping them down* to the $A(T,V,x_1,x_2,N)$ variable set—the asymmetric ternary Helmholtz function—which is compatible with pressure-explicit mixture equations such as the Peng−Robinson equation. For those cases where *experimental data* are available (and indexed on temperature, *pressure*, and composition), the $G(T,P,x_1,x_2,N)$ set corresponding to Figure 15 would be the proper choice. The analogous step-down operation for a binary mixture is shown by eq 21. This procedure is demonstrated in refs 22 and 25.

For a final example, we move to Figure 18 and a fourth $(n+1)$th transform, with symmetric variables, volume scaling,

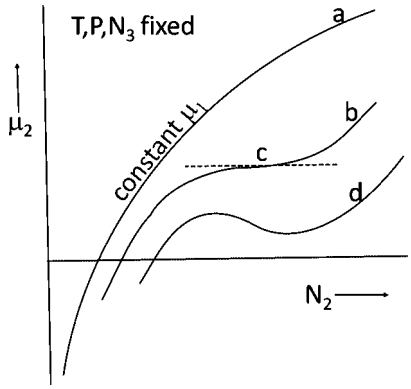

Figure 19. Isothermal, isobaric, constant-μ_1 curves for a ternary mixture (1−2−3) near a critical point c. Adapted from Prigogine and Defay.[39]

differencing, and with temperature with one chemical potential held constant at values that, again, give the equimolar critical point.

$$A'''d_v = f(\mu_2, \mu_3)_{T,\mu_1} \tag{22}$$

The swallowtail appears as expected, and, again, the unstable cap is omitted for visibility but implied by three folded-back red lines. The overlaid red and green crosses appear as in the dissertation[20] to indicate that the blue (stable) regions represent vapor to the left and liquid to the right. As previously stated, the metastable sections (transparent yellow sheets) are extensions of the stable regions beyond their intersection along the coexistence curve.

One can show that the dependent variable here is the reduced, differenced, negative of the pressure. Thus, the coexistence curve in Figure 18 may be considered to give the monovariant saturation pressure for the ternary when both phases are present, the temperature and $\mu_{C_2H_4}$ are fixed, and either $\mu_{n\text{-}C_4H_{10}}$ or μ_{CO_2} is taken to be the independent variable. The nature of these five quantities assures phase equilibrium at all points along the curve of self-intersection.

For a ternary EOS, the reader is referred to the Gibbs website, where two forms are shown (*Index of drawings, Ternary Equations of State*): Referring to the Web figure captions, one is the derivative of the asymmetric third transform G^+ [with the heading $(\eta_2 x_2 \eta_1)_{T,P}$]. In Figure 19, we show a classic sketch, again adapted from Prigogine and Defay,[39] in which curves of constant μ_1 are plotted against the mole ratio N_2/N_3 to give the behavior of μ_2. The subcritical curve d shows the familiar minimum/maximum characteristics. If Figure 19 had been drawn in terms of mole-fraction compositions and modified chemical potentials, it would be a precise match to the derivative of the G^+ form shown on the website.

In Conclusion

We have presented computer-drawn images of a sampling of the many Legendre-transformed functions from which the working expressions of the macroscopic thermodynamics of equilibrium (MTE) are derived. We have used a variety of graphics tools to make the drawings visually convincing, and we have given explanations that we hope will help the viewer connect those geometries with the constrained systems that they represent. But we are not the first thermodynamicists with questioning eyes to ponder the structures and inter-relationships that exist among these interesting physical−chemical−mathematical forms. Over the decades, they have gained the attention of a small but important segment of the thermodynamics cognoscenti.

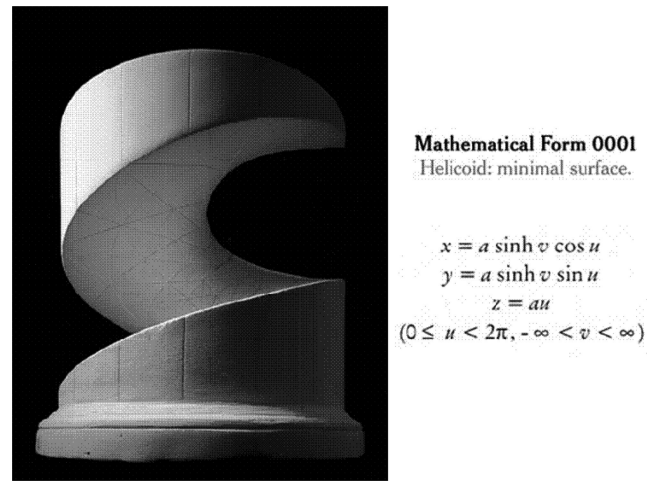

Figure 20. Mathematical sculpture photographed by Sugimoto.[46] [From *The New York Times*, December 2, 2004. Copyright 2004, The New York Times (www.nytimes.com). All rights reserved. Used by permission and protected by the Copyright Laws of the United States. The printing, copying, redistribution, or retransmission of the Material without express written permission is prohibited.]

We recall the beautiful work of Heike Kamerlingh Onnes, a physicist at the University of Leiden and a 1913 Nobel Laureate for his work to liquefy helium.[41,42] Kamerlingh Onnes also was interested in the thermodynamics of fluids, and he understood the power of visual thinking very well. With his colleagues and students, he coauthored a group of papers in the early 1900s where not only were the properties of pure fluids and mixtures examined, but the results of the studies cast into elegant, three-dimensional, Gibbs−Maxwell-like models.[43] In her overview of the Dutch School of thermodynamics,[44,45] Anneke Sengers noted that most of the Kamerlingh Onnes models have been preserved at the Boerhaave Museum at Leiden.

We are reminded also of Hiroshi Sugimoto's dramatic photographs of stereometric models made of plaster and used in turn-of-the century Germany to help scholars grasp complex mathematical formulas.[46] We show one in Figure 20. In Sugimoto's words, "Art is possible even without artistic intention".

But the skeptic may still ask:

"Why drawings?"

"Aren't words and numbers enough?"

"Why mix exact science with subjective art?"

"Why not just calculate these quantities and be done with it?"

"What good are qualitative sketches and geometric procedures when a scientist or engineer may ultimately need results accurate to within a few tenths of a percent?"

"Isn't that what computers and precision instruments are for?"

We counter by claiming that many who have tackled this onerous subject over the 135 years since J. Willard Gibbs gave it formal life have tried to do so exactly that way: *by the numbers*. The organization, the transformations, and the interconnections discussed in this paper have frequently not been emphasized. Too often, conventional pedagogy has encouraged rote memorization of ill-connected facts, with the results being forced definitions and circular arguments. No professional thermodynamicist should be surprised to hear the subject spoken of among the rank and file as *abstract* and *incomprehensible*.

Our visual models offer a tangible middle ground—a halfway house between barren mathematical formulas and the painfully slow and scrupulously demanding experiments that can support

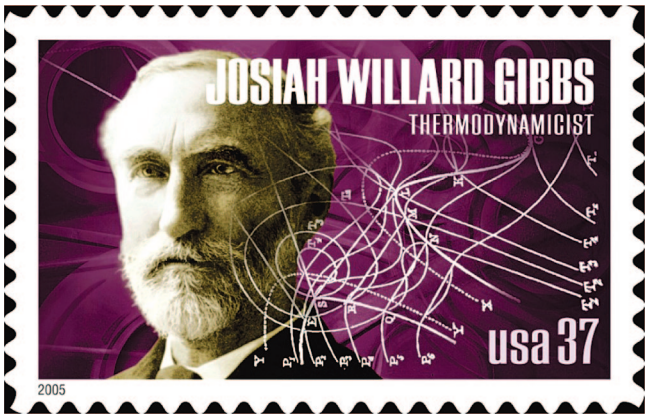

Figure 21. The J. W. Gibbs Commemorative postage stamp for 2005.[50] Author K.R.J. was scientific consultant to the U.S. Postal Service for design of the stamp. Gibbs' *signature expression,* $d\varepsilon = t\,d\eta - p\,dv$, appears on the manufactured stamps and may be seen with the help of high magnification on the collar of Gibbs' shirt.[51] (Josiah Willard Gibbs Stamp Design, Copyright 2005, United States Postal Service. All Rights Reserved. Used with permission.)

most of the claims of classical thermodynamics. When faced with exactly that range of choices, the cautious engineer most often opts for the center position, and that is what we hope our readers will choose.

We began this paper by recalling J. C. Maxwell's first words about the merits of Gibbs' "exceedingly valuable method of studying the properties of a substance by means of a surface". We end by noting the special significance of those words following the release of four first-class U.S. postage stamps to commemorate Gibbs and three other American scientists.[47] The Gibbs stamp is shown in Figure 21, and on it we see the map of the famous Maxwell model, an early and powerful example of science visualized through art.[48] The time is upon us to use that art and our magnificent modern graphics tools to show scientific ideas visually and to have pictures become the equal of numbers in dialogue among educated people.

A Word About the Graphics

The computer drawings in this paper were made in the early 1990s using the type of hardware and software commonly available to academic engineering departments at the time. The programs that generated the property data and that organized those data into the combinations of arrays needed for graphics rendering were unique in their ability to handle the special geometries of thermodynamic fundamental and state functions.[20] Partitioning the surfaces into stability-based, colored zones, with precise boundaries, was a tedious computing operation in itself.

The rendering was done by the then-popular solid-modeling package, MOVIE BYU, which is a software product that was developed by Professor Henry Christiansen in the Department of Civil Engineering at Brigham Young University.[49] We gratefully acknowledge the help of Dr. Christiansen and his co-workers.

Computer graphics has progressed very far in the 15 years since these images were constructed. Memories are larger, computing speeds are faster, and newer utilities such as surface clipping and ease of animation might now reduce the work required to create them, as well as improve the ways in which they are viewed. However, the personal effort needed to move from basic thermodynamic data sources to finished geometry files of transformed variables would be about as great today as it was when the research was done. Computer visualization, when well-conceived, should delight its viewers but also insulate them from the intense labor needed to produce it.

Acknowledgment

Wendy Ortmann managed the manuscript. Linda Edson modified the computer drawings and created Figures 16 and 19. William Beach created Figure 13, as noted earlier. Wenqing Li (Pfizer, Inc.) programmed the graphics for Figure 2. Michael McBride (Yale University) photographed the Gibbs/Maxwell model. John Ouart (Iowa State) programmed the Gibbs Models Website. Scott Munhall (ATK-Thiokol) assisted with the calculations. Financial support at Iowa State University came from the Chemical and Biological Engineering Department, from a Miller Faculty Fellowship to K.R.J., and from a Publication Subvention grant from the Office of the Vice President for Research. Additional support was provided by the General Electric Foundation. Graphics facilities were funded in part by the National Science Foundation. D.C.C. received an Amoco Foundation Doctoral Fellowship.

Supporting Information Available: The mathematical analysis and the resulting equations used to produce data for the Gibbs models are provided as Supporting Information. (PDF) This material is available free of charge via the Internet at http://pubs.acs.org.

Literature Cited

(1) Aristotle. *De Anima*; Bk. *III, 431a*, pp 15−17.

(2) West, T. G. *In the Mind's Eye*; Prometheus Books: Buffalo, NY, 1991; Chapters 4 and 6.

(3) Greenburg, D.; Marcus, A.; Schmidt, A.; Gorter, V. *The Computer Image: Applications of Computer Graphics*: Addison−Wesley: Reading, MA, 1982.

(4) Jolls, K. R. The Visual Side of Science. *The New York Times, Science* **2007**, (June 19, Letters), D4.

(5) Jolls, K. R. Left Brain, Right Brain. *The New York Times, Business* **2008**, (April 13, Letters), Bu 6.

(6) Gibbs, J. W. Graphical Methods in the Thermodynamics of Fluids. *Trans. Conn. Acad.* **1873**, *II* (Part 2, Art. XI), 309–342.

(7) Gibbs, J. W. A Method of Geometrical Representation of the Thermodynamic Properties of Substances by Mean of Surfaces. *Trans. Conn. Acad.* **1873**, *II* (Part 2, Art. XIV), 382–404.

(8) (a) Gibbs, J. W. On the Equilibrium of Heterogeneous Substances (first part). *Trans. Conn. Acad.* **1875**, *III* (Art. V), 108–248. (b) Gibbs, J. W. On the Equilibrium of Heterogeneous Substances (concluded). *Trans. Conn. Acad.* **1877**, *III* (Art. X), 343–524.

(9) Maxwell, J. C. *Theory of Heat*, 4th Edition; Longmans, Green, and Co.: London, 1875; pp 195−208.

(10) Clark, A. L.; Katz, L. Thermodynamic Surfaces of H_2O. *Trans. R. Soc. Can., Sect. III* **1939**, *33*, 59.

(11) Wheeler, L. P. *Josiah Willard Gibbs: The History of a Great Mind*; Yale University Press: New Haven, CT, 1951.

(12) Jolls, K. R. Gibbs and the Art of Thermodynamics. In *Proceedings of the Gibbs Symposium*; Mostow, G. D., Caldi, D. G., Eds.; American Mathematical Society: Providence, RI, 1990; p 293.

(13) (a) Kestin, J. *A Course in Thermodynamics*; Blaisdel: Waltham, MA, 1966; Vol. I, pp 80, 295, 296, 300, 314, 318. (b) Kestin, J. *A Course in Thermodynamics*; Blaisdel: Waltham, MA, 1966; Vol. II, pp 13, 277, 288, 337, 339.

(14) Tamás, F.; Pál, I. *Phase Equilibria Spatial Diagrams, Their Interpretation and Anaglyph Representation* (translated from Hungarian by F. Tamás); Iliffe Books, Ltd.: London, 1970.

(15) Sears, F. W. *An Introduction to Thermodynamics: The Kinetic Theory of Gases, and Statistical Mechanics*, 2nd Edition; Addison−Wesley: Reading, MA, 1953; pp 19, 21, 64, 65, 89, 90, 94, 99, 157, 158, 183, 190.

(16) Charos, G. N.; Clancy, P.; Gubbins, K. E. Three dimensional *PTx* phase diagrams through interactive computer graphics. *Fluid Phase Equilib.* **1985**, *23* (1), 59–78.

(17) Picard, D. *Thermodynamic Diagrams for Pure Fluids*; Union des Professeurs de Physique et de Chemie: Paris, 2007; Vol. 101, p 587.

(18) Jolls, K. R. Keeping Eyes Open. *The New York Times, Arts and Leisure* **2001**, (May 6, Letters), AR4.

(19) Peng, D.-Y.; Robinson, D. B. A New Two-Constant Equation of State. *Ind. Eng. Chem. Fundam.* **1976**, *15*, 59.

(20) Coy, D. C. Visualizing thermodynamic stability and phase equilibrium through computer graphics, Ph.D. dissertation, Department of Chemical Engineering, Iowa State University, Ames, IA, 1993.

(21) Tisza, L. Personal communication.

(22) Modell, M.; Reid, R. C. *Thermodynamics and Its Applications*, Second Edition; Prentice Hall: Englewood Cliffs, NJ, 1983.

(23) Callen, H. B. *Thermodynamics and an Introduction to Thermostatistics*, 2nd Edition; Wiley: Hoboken, NJ, 1985.

(24) Alberty, R. A. Legendre Transforms in Chemical Thermodynamics. *Chem. Rev.* **1994**, *94* (6), 1457–1482.

(25) O'Connell, J. P.; Haile, J. M. *Thermodynamics: Fundamentals for Application*; Cambridge University Press: Oxford, U.K., 2005.

(26) Honig, J. M. *Thermodynamics*, 3rd Edition; Academic Press: New York, 2007; p 106.

(27) Massieu, M. F. Sur les fonctions caractéristiques des divers fluides. *Comptes Rendus* **1869**, *69*, 858, 1057.

(28) Clausius, R. Über verschiedene für die Anwendung bequeme Formen der Hauptgleichungen der mechanischen Wärmetheorie. *Ann. Phys. (Weinheim, Ger.)* **1865**, *125*, 400 (English version: Clausius, R. *The Mechanical Theory of Heat*, translated by J. Tyndall; John van Voorst: London, 1867; p 365.)

(29) Gilmore, R. *Catastrophe Theory for Scientists and Engineers*; Wiley: New York, 1981; Chapter 10.

(30) (a) Reid, R. C. Superheated Liquids: A Laboratory Curiosity and, Possibly, an Industrial Curse. *Chem. Eng. Ed.* **1978**, *12* (2), 60. (b) Reid, R. C. Superheated Liquids: A Laboratory Curiosity and, Possibly, an Industrial Curse. *Chem. Eng. Ed.* **1978**, *12* (3), 108. (c) Reid, R. C. Superheated Liquids: A Laboratory Curiosity and, Possibly, an Industrial Curse. *Chem. Eng. Ed.* **1978**, *12* (4), 194.

(31) Modell, M.; Tester, J. W. *Thermodynamics and Its Applications*, 3rd Edition; Prentice Hall: Englewood Cliffs, NJ, 1996.

(32) Jolls, K. R.; Butterbaugh, J. L. Confirming Thermodynamic Stability: A Classroom Example. *Chem. Eng. Ed.* **1992**, 124.

(33) Elliott, J. R.; Lira, C. T. *Introductory Chemical Engineering Thermodynamics*; Prentice Hall: Upper Saddle River, NJ, 1999; p 273.

(34) Lupis, C. H. P. *Chemical Thermodynamics of Materials*; North−Holland: New York, 1983.

(35) Smith, J. M.; Van Ness, H. C.; Abbott, M. M *Introduction to Chemical Engineering Thermodynamics*, 5th Edition; McGraw−Hill: New York, 1996.

(36) http://mathworld.wolfram.com/CuspCatastrophe.html.

(37) Prausnitz, J. M.; Lichtenthaler, R. U.; Gomez de Azevedo, E. *Molecular Thermodynamics of Fluid-Phase Equilibria*, 2nd Edition; Prentice Hall: Englewood Cliffs, NJ, 1986.

(38) Tisza, L. *Generalized Thermodynamics*; MIT Press: Cambridge, MA, 1966.

(39) Prigogine, I.; Defay, R. *Chemical Thermodynamics*. (translated by D. H. Everett); Longmans, Green, and Co.: London, 1954.

(40) Holmes, A. S.; Ryan, J. M. Distillative separation of carbon dioxide from light hydrocarbons, U.S. Patent 4,350,511, 1982.

(41) Gavroglu, K. ; Gondarolis, Y. Through Measurement to Knowledge: The Selected Papers of Heike Kamerlingh Onnes, 1853−1926. In *Boston Studies in the Philosophy of Science*, Vol. 124; Kluwer Academic Publishers: Dordrecht, The Netherlands, 1991.

(42) http://nobelprize.org/physics/laureates/1913/onnes-bio.html.

(43) Kamerlingh Onnes, H.; Jolles, T. C. Contributions to the knowledge of the Ψ-surface of Van Der Waals, XIV. Graphical deduction of the results of Kuenen's experiments on mixtures of ethane and nitrous oxide *Commun. Phys. Lab. Univ. Leiden*, **1907** (Suppl. No. 14), 85–96. [The relationship of author T. C. Jolles to the present author is unknown but possible through common Dutch ancestry.]

(44) http://www.knaw.nl/waals/.

(45) Levelt Sengers, J. M. H. *How fluids unmix: Discoveries by the School of Van der Waals and Kamerlingh Onnes*; Royal Netherlands Academy of Arts and Sciences: London, 2002.

(46) Sugimoto, H. Reimagined Math. *The New York Times Magazine* **2004**, (Dec. 5), 56.

(47) Yours for 37 Cents: Lifetimes of Discovery. *The New York Times, Science* **2005**, (March 15), F2.

(48) Jolls, K. R. Computer models can help explain thermodynamics. *The New Haven Register (Letters)* **2005**, (June 19), B2.

(49) A General Purpose Computer Graphics System, operating guide for MOVIE BYU, version 6; Department of Civil Engineering, Brigham Young University: Provo, UT, 1987.

(50) *The 2005 Commemorative Stamp Yearbook*; United States Postal Service: Washington, DC, 2005; p 22.

(51) Spakovszky, Z. Stamp of Authenticity. *Mech. Eng. (Am. Soc. Mech. Eng.).* **2006**, *128* (4, Letters), 8.

Received for review September 21, 2007
Revised manuscript received June 9, 2008
Accepted June 10, 2008

IE071277B